

An implicit split-operator algorithm for the nonlinear time-dependent Schrödinger equation

Julien Roulet^{a)} and Jiří Vaníček^{b)}

Laboratory of theoretical physical chemistry, Institut des sciences et ingénieries Chimiques, Ecole Polytechnique Fédérale de Lausanne (EPFL), Lausanne, Switzerland

(Dated: 12 November 2021)

The explicit split-operator algorithm is often used for solving the linear and nonlinear time-dependent Schrödinger equations. However, when applied to certain nonlinear time-dependent Schrödinger equations, this algorithm loses time reversibility and second-order accuracy, which makes it very inefficient. Here, we propose to overcome the limitations of the explicit split-operator algorithm by abandoning its explicit nature. We describe a family of high-order implicit split-operator algorithms that are norm-conserving, time-reversible, and very efficient. The geometric properties of the integrators are proven analytically and demonstrated numerically on the local control of a two-dimensional model of retinal. Although they are only applicable to separable Hamiltonians, the implicit split-operator algorithms are, in this setting, more efficient than the recently proposed integrators based on the implicit midpoint method.

I. INTRODUCTION

The nonlinear time-dependent Schrödinger equation (NL-TDSE) appears in the approximate treatment of many physical processes, where the approximate Hamiltonian depends on the state of the system. This happens, e.g., in approximations generated by the Dirac-Frenkel variational principle,^{1–4} such as the multiconfigurational time-dependent Hartree method,^{5–7} variational Gaussian approximation,^{8,9} and variational multiconfigurational Gaussian method,^{10,11} or in methods based on local expansion of the potential, such as the thawed Gaussian approximation,^{12–14} Hagedorn wavepacket method,^{9,15,16} or single Hessian approximation.^{17,18} In addition, many numerical methods for solving the linear Schrödinger equation, such as the short-iterative Lanczos algorithm,^{19–21} can be interpreted as exact solutions of an effective NL-TDSE.

The best known NL-TDSE is the Gross-Pitaevskii equation,^{22–26} which models the dynamics of Bose-Einstein condensates.^{27,28} To solve this NL-TDSE with cubic nonlinearity, the explicit second-order split-operator algorithm^{29–32} is frequently used³³ because it is efficient and geometric.³⁴ However, we recently showed³⁵ that the success of the explicit split-operator algorithm in solving this NL-TDSE is due to its simple nonlinearity and, therefore, is rather an exception than a rule. Indeed, for other nonlinearities, the algorithm becomes time-irreversible and inefficient because its accuracy decreases to the first order in the time step.³⁵ In many applications, this is not an issue, but it can become a problem if accurate wavefunctions are needed.

As we have recently demonstrated,³⁵ an example of a NL-TDSE, on which the split-operator algorithm loses the second-order accuracy and time reversibility, is pro-

vided by local control theory (LCT).^{36–46} LCT is a technique that aims at controlling the expectation value of a specified operator by computing, from the state, an electric field that will either increase or decrease the chosen expectation value. Because the electric field is state-dependent, the interaction between this electric field and the system is nonlinear.

To overcome the limitations of the explicit split-operator algorithm applied to general NL-TDSEs, in our previous work³⁵ we developed high-order integrators by symmetrically composing the implicit midpoint method. These integrators are applicable to the general nonlinear Schrödinger equation with both separable and non-separable Hamiltonians and, in contrast to the explicit split-operator algorithm, are efficient, while preserving the geometric properties of the exact solution.

Here, we show that it is not necessary to abandon the split-operator algorithm altogether, but only its explicit nature. In the linear case, the second-order split-operator algorithms are obtained by composing two adjoint first-order split-operator methods, which are both explicit. We show that to achieve a second-order accuracy in the nonlinear case, one of the two adjoint algorithms must be implicit. Although implicit generalizations of the Verlet algorithm exist^{47–50} for classical systems with non-separable Hamiltonians, to the best of our knowledge no implicit splitting methods were developed for quantum systems with separable but nonlinear Hamiltonians. Therefore, we present an implicit generalization of the second-order split-operator algorithm, which is geometric, applicable to the general NL-TDSE, and can be composed with various composition methods^{51–54} to further increase its order of convergence and efficiency.

The remainder of this paper is organized as follows: In Sec. II, we present the NL-TDSE, discuss the geometric properties of its evolution operator and describe how LCT generates a NL-TDSE. In Sec. III, we present the algorithms, their geometric properties and the procedure employed to perform the implicit propagation required in the implicit split-operator algorithms. In Sec. IV, we

^{a)}Electronic mail: julien.roulet@epfl.ch

^{b)}Electronic mail: jiri.vanicek@epfl.ch

verify the convergence and the geometric properties of the proposed integrators by performing LCT on a two-dimensional model of retinal. Section V concludes this work.

II. NONLINEAR SCHRÖDINGER EQUATION

The *nonlinear time-dependent Schrödinger equation*

$$i\hbar \frac{d}{dt} |\psi_t\rangle = \hat{H}(\psi_t) |\psi_t\rangle \quad (1)$$

describes the time evolution of the molecular state ψ_t under the influence of a state-dependent Hamiltonian operator $\hat{H}(\psi_t)$. We will assume that the Hamiltonian

$$\hat{H}(\psi) := T(\hat{p}) + V_{\text{tot}}(\hat{q}, \psi) \quad (2)$$

is separable into a sum of a momentum-dependent kinetic energy operator $T(\hat{p})$ and a position-dependent nonlinear potential energy operator $V_{\text{tot}}(\hat{q}, \psi)$, with \hat{p} and \hat{q} denoting the momentum and position operators, respectively.

A. Geometric properties of the exact evolution operator

The formal solution of Eq. (1) with initial condition ψ_{t_0} can be expressed as

$$|\psi_t\rangle = \hat{U}(t, t_0; \psi) |\psi_{t_0}\rangle, \quad t \geq t_0, \quad (3)$$

where the exact evolution operator \hat{U} is given by the time-ordered exponential

$$\hat{U}(t, t_0; \psi) = \mathcal{T} \exp \left[-\frac{i}{\hbar} \int_{t_0}^t dt' \hat{H}(\psi_{t'}) \right], \quad (4)$$

with \mathcal{T} denoting the time-ordering operator. Because the Hamiltonian in Eq. (1) is nonlinear, the exact evolution operator (4) is also nonlinear; we emphasize this by including ψ as an explicit argument of \hat{U} . When solving Eq. (1), some geometric properties conserved by the linear time-dependent Schrödinger equation are not conserved in the nonlinear case. The exact nonlinear evolution operator (4) does not conserve the inner product and, as a result, is not symplectic.³⁵ Furthermore, the energy is not conserved because the state dependence of the Hamiltonian makes it implicitly time-dependent. However, we demonstrated that the exact nonlinear evolution operator conserves the norm and is time-reversible.³⁵

B. Nonlinear Hamiltonian of local control theory

Local control theory^{36,37} aims at controlling the expectation value $\langle \hat{O} \rangle_{\psi_t} := \langle \psi_t | \hat{O} | \psi_t \rangle$ of a chosen operator \hat{O} in the state ψ_t . To this end, a state-dependent electric

field $\vec{E}_{\text{LCT}}(\psi_t)$ is computed on the fly so that the expectation value $\langle \hat{O} \rangle_{\psi_t}$ increases or decreases monotonously when the electric field interacts with the system. Within the electric-dipole approximation,⁵⁵ this interaction is described by the interaction potential

$$\hat{V}_{\text{LCT}}(\psi_t) := -\hat{\vec{\mu}} \cdot \vec{E}_{\text{LCT}}(\psi_t), \quad (5)$$

where $\hat{\vec{\mu}}$ is the electric dipole moment operator. Due to the state-dependent control field, both the operator (5) and the total potential energy operator $\hat{V}_{\text{tot}}(\psi) := \hat{V}_0 + \hat{V}_{\text{LCT}}(\psi)$ [see Eq. (2)], where \hat{V}_0 denotes the molecular potential energy operator, are nonlinear. To control the expectation value $\langle \hat{O} \rangle_{\psi_t}$, the control field used in Eq. (5) is computed as

$$\vec{E}_{\text{LCT}}(\psi_t) := \pm \lambda i \langle [\hat{\vec{\mu}}, \hat{O}] \rangle_{\psi_t}^* = \mp \lambda i \langle [\hat{\vec{\mu}}, \hat{O}] \rangle_{\psi_t}, \quad (6)$$

where $\lambda > 0$ is a parameter that scales the amplitude of the control field and the sign is chosen according to whether one wants to increase or decrease $\langle \hat{O} \rangle_{\psi_t}$. The control field (6) ensures³⁵⁻³⁷ that the time derivative $d\langle \hat{O} \rangle_{\psi_t}/dt$ remains positive [or negative, depending on the sign in Eq. (6)], indicating a monotonic evolution of $\langle \hat{O} \rangle_{\psi_t}$. However, this monotonic behavior is only guaranteed if the chosen operator \hat{O} commutes with the unperturbed molecular Hamiltonian $\hat{H}_0 := \hat{T} + \hat{V}_0$, i.e., if $[\hat{O}, \hat{H}_0] = 0$.^{35,38,44}

III. GEOMETRIC INTEGRATORS FOR THE NONLINEAR TIME-DEPENDENT SCHRÖDINGER EQUATION

To solve the NL-TDSE (1), numerical propagation methods obtain the state $\psi_{t+\Delta t}$ at time $t + \Delta t$ from the state ψ_t at time t using the relation

$$|\psi_{t+\Delta t}\rangle = \hat{U}_{\text{appr}}(t + \Delta t, t; \psi) |\psi_t\rangle, \quad (7)$$

where $\hat{U}_{\text{appr}}(t + \Delta t, t; \psi)$ denotes an approximate evolution operator which depends on ψ and where Δt is the numerical time step. While all reasonable numerical methods give the exact solution in the limit $\Delta t \rightarrow 0$, some geometric properties of the exact evolution operator may not be preserved by the numerical methods using a finite Δt . In this section, we present the different numerical methods and discuss their geometric properties. Detailed proofs of the geometric properties of the presented numerical methods are shown in Appendix A.

A. Loss of geometric properties by the first-order split-operator algorithms

For separable Hamiltonians, the simplest split-step methods are the *explicit TV* and *implicit VT* split-

operator algorithms, which approximate the exact evolution operator, respectively, as

$$\hat{U}_{\text{TV}}(t + \Delta t, t; \psi_t) := \hat{U}_{\hat{T}}(\Delta t) \hat{U}_{\hat{V}_{\text{tot}}(\psi_t)}(\Delta t), \quad (8)$$

$$\hat{U}_{\text{VT}}(t + \Delta t, t; \psi_{t+\Delta t}) := \hat{U}_{\hat{V}_{\text{tot}}(\psi_{t+\Delta t})}(\Delta t) \hat{U}_{\hat{T}}(\Delta t), \quad (9)$$

where $\hat{U}_{\hat{A}}(\Delta t) := e^{-i\hat{A}\Delta t/\hbar}$ denotes an evolution operator associated with a time-independent Hermitian operator \hat{A} and time step Δt . Both integrators (8) and (9) are norm-conserving. However, both lose the symmetry and time reversibility of the exact evolution operator. Moreover, both integrators are only first-order accurate in the time step, and therefore, very inefficient. Note also that the TV split-operator algorithm is explicit because it depends on the state ψ_t while the VT split-operator algorithm is, due to its dependence on the state $\psi_{t+\Delta t}$, implicit and, therefore, requires solving a nonlinear system of equations.

B. Recovery of geometric properties and increasing accuracy by composition

Because the integrators (8) and (9) are adjoints of each other (see Appendix A 2 for more details), they can be composed together to obtain the *implicit TVT* algorithm

$$\begin{aligned} \hat{U}_{\text{TVT}}(t + \Delta t, t; \psi_{t+\Delta t/2}) \\ := \hat{U}_{\text{TV}}(t + \Delta t, t + \Delta t/2; \psi_{t+\Delta t/2}) \\ \times \hat{U}_{\text{VT}}(t + \Delta t/2, t; \psi_{t+\Delta t/2}) \end{aligned} \quad (10)$$

or the *implicit VTV* algorithm

$$\begin{aligned} \hat{U}_{\text{VTV}}(t + \Delta t, t; \psi) \\ := \hat{U}_{\text{VT}}(t + \Delta t, t + \Delta t/2; \psi_{t+\Delta t}) \\ \times \hat{U}_{\text{TV}}(t + \Delta t/2, t; \psi_t), \end{aligned} \quad (11)$$

depending on the order of composition. Both of these integrators are second-order accurate in the time step and geometric because they preserve all the geometric properties of the exact evolution operator, i.e., they are norm-conserving, symmetric, and time-reversible. However, since both rely on the implicit VT split-operator algorithm, both are implicit methods.

We will compare the properties of the VTV and TVT methods with the second-order accurate *implicit midpoint* method

$$\begin{aligned} \hat{U}_{\text{mid}}(t + \Delta t, t; \psi_{t+\Delta t/2}) \\ := \hat{U}_{\text{expl}}(t + \Delta t, t + \Delta t/2; \psi_{t+\Delta t/2}) \\ \times \hat{U}_{\text{impl}}(t + \Delta t/2, t; \psi_{t+\Delta t/2}), \end{aligned} \quad (12)$$

which is also geometric, and can, in contrast to the implicit TVT and VTV split-operator algorithms, be used for both separable and nonseparable Hamiltonians.

The implicit midpoint method is obtained by composing the first-order accurate *explicit* $\hat{U}_{\text{expl}}(t + \Delta t, t; \psi_t) := 1 - i\hat{H}(\psi_t)\Delta t/\hbar$ and *implicit* $\hat{U}_{\text{impl}}(t + \Delta t, t; \psi_{t+\Delta t}) := [1 + i\hat{H}(\psi_{t+\Delta t})\Delta t/\hbar]^{-1}$ Euler methods, which are adjoints of each other. For a detailed description of the implicit midpoint and Euler methods in the context of NL-TDSEs, we refer the reader to Ref. 35.

The second-order methods (10)-(12) are all symmetric and time-reversible regardless of the size of the time step. Therefore, they can be further composed using symmetric composition methods^{34,35,49-54,56,57} in order to obtain integrators of arbitrary even orders of convergence. To this end, starting from an integrator \hat{U}_p of even order p , an integrator \hat{U}_{p+2} of order $p+2$ is generated using the symmetric composition

$$\begin{aligned} \hat{U}_{p+2}(t + \Delta t, t; \psi) := \hat{U}_p(t + \xi_M \Delta t, t + \xi_{M-1} \Delta t; \psi) \\ \cdots \hat{U}_p(t + \xi_1 \Delta t, t; \psi), \end{aligned}$$

where $\xi_n := \sum_{j=1}^n \gamma_j$ is the sum of the first n real composition coefficients γ_j and M denotes the total number of composition steps. Composition coefficients $\gamma_1, \dots, \gamma_M$ satisfy the relations $\sum_{n=1}^M \gamma_n = 1$ (consistency), $\gamma_{M+1-n} = \gamma_n$ (symmetry), and $\sum_{j=1}^M \gamma_j^{p+1} = 0$ (order increase).⁵⁰ In this work, we will use the triple-jump⁵¹ ($M = 3$) and Suzuki's fractal⁵² ($M = 5$) composition methods, which can both generate integrators of arbitrary even orders of convergence. However, the number of composition steps increases exponentially with the order of convergence, increasing drastically the cost of performing a single time step. To circumvent this, we will also use nonrecursive methods^{53,54} for obtaining sixth- eight- and tenth-order integrators. These composition methods, which will be referred to as "optimal", were designed so that they minimize either the sum $\sum_{n=1}^M |\gamma_n|$ or the maximum $\max_n |\gamma_n|$ of the magnitudes of the composition steps and, therefore, are more efficient than both the triple-jump and Suzuki's fractal. For more details on these composition methods, see Ref. 57. Note that by "order" we mean the formal order because, as shown by Lubich⁵⁸ and Thalhammer,⁵⁹ who performed rigorous convergence analysis of splitting methods applied to the NL-TDSE, the actual order depends on the regularity of the initial state. Because we do not perform this analysis here, we will verify the predicted (formal) order numerically in Sec. IV.

C. Approximate application of the explicit split-operator algorithm

Because implicit algorithms require more expensive iterative solvers, it is tempting to ignore the implicit character of the above-described VTV and TVT algorithms, and instead employ their explicit versions, which consist of using the state ψ that is available for computing the evolution operator for \hat{V}_{tot} . For example, instead

of using the state $\psi_{t+\Delta t}$ in Eq. (9) (i.e., performing the implicit propagation exactly for the VT algorithm), the state $\psi_{\hat{T},\Delta t/2} := \hat{U}_{\hat{T}}(\Delta t/2)\psi_t$ obtained after the kinetic propagation is often used. After composition with the TV algorithm, this yields the *approximate explicit TVT* algorithm

$$\begin{aligned} \hat{U}_{\text{expl TVT}}(t + \Delta t, t; \psi_{t,\hat{T}\Delta t/2}) \\ := \hat{U}_{\text{TV}}(t + \Delta t, t + \Delta t/2; \psi_{t,\hat{T}\Delta t/2}) \\ \times \hat{U}_{\text{VT}}(t + \Delta t/2, t; \psi_{t,\hat{T}\Delta t/2}). \end{aligned} \quad (13)$$

This approximate integrator can be used for performing practical LCT calculations in typical situations, which do not require high accuracy.^{41,42,44–46} However, despite conserving the norm, the integrator is only first-order accurate and neither symmetric nor time-reversible, as shown in Ref. 35. Indeed, any explicit version of the integrators (10) and (11) will be first-order accurate and time-irreversible due to ignoring the implicit character of the VT algorithm.

D. Solving the implicit propagation

Both TVT and VTV implicit split-operator algorithms rely on the implicit VT method. Using the evolution operator \hat{U}_{VT} from Eq. (9), the implicit VT propagation of a state $|\psi_t\rangle$ is translated into solving the nonlinear system

$$\hat{U}_{\text{VT}}(t + \Delta t, t; \psi_{t+\Delta t})^{-1}|\psi_{t+\Delta t}\rangle = |\psi_t\rangle. \quad (14)$$

This nonlinear system can be written as $f(\psi_{t+\Delta t}) = 0$ with the nonlinear functional

$$\begin{aligned} f(\psi) &:= \hat{U}_{\hat{T}}(\Delta t)[\hat{U}_{\text{VT}}(t + \Delta t, t; \psi)^{-1}\psi - \psi_t] \\ &= \hat{U}_{\hat{T}}(\Delta t)[\hat{U}_{\hat{T}}(\Delta t)^{-1}\hat{U}_{\hat{V}_{\text{tot}}}(\Delta t)^{-1}\psi - \psi_t] \\ &= \hat{U}_{\hat{V}_{\text{tot}}}(\Delta t)^{-1}\psi - \hat{U}_{\hat{T}}(\Delta t)\psi_t, \end{aligned} \quad (15)$$

where we have, for convenience, included a nonzero factor of $\hat{U}_{\hat{T}}(\Delta t)$ into the definition of $f(\psi)$.

Following Ref. 35, we employed the Newton-Raphson method to solve this nonlinear system. This method computes, until convergence, iterative solutions of the nonlinear system using the iterative map

$$\psi^{(k+1)} = \psi^{(k)} + \delta\psi^{(k)} \quad (16)$$

where $\psi^{(k)}$ denotes the solution obtained at the k th iteration and $\delta\psi^{(k)}$ is the state obtained by solving the linear system

$$\hat{J}(\psi^{(k)})\delta\psi^{(k)} = -f(\psi^{(k)}), \quad (17)$$

with $\hat{J} := \delta f(\psi)/\delta\psi$ denoting the Jacobian of the nonlinear mapping $f(\psi)$. The linear system (17) is solved using the generalized minimal residual method,^{60–62} an

iterative method based on the Arnoldi process^{63,64} (see the supplementary material of Ref. 35 for a detailed presentation of this algorithm). Similarly to Ref. 35, we employ the solution from the explicit propagation, i.e., the solution obtained using Eq. (8), as the initial guess $\psi^{(0)}$. However, if the initial guess is too far from the implicit solution, which happens at large time steps, the algorithm fails to converge.

The procedure described above differs from that presented in Ref. 35 only by the nonlinear system one needs to solve. Fortunately, the use of approximations for estimating the Jacobian is, as in Ref. 35, avoided because the Jacobian $\hat{J}(\psi)$ of the nonlinear function (15) can be obtained analytically:

$$\begin{aligned} \hat{J}(\psi) &= \frac{\delta}{\delta\psi} \left[\hat{U}_{\hat{V}_{\text{tot}}}(\Delta t)^{-1}\psi \right] \\ &= \frac{\delta}{\delta\psi} \left[\hat{U}_{\hat{V}_{\text{tot}}}(\Delta t)^{-1} \right] \psi + \hat{U}_{\hat{V}_{\text{tot}}}(\Delta t)^{-1}\hat{1} \\ &= \frac{i}{\hbar} \Delta t \hat{U}_{\hat{V}_{\text{tot}}}(\Delta t)^{-1} \frac{\delta}{\delta\psi} \left[\hat{V}_{\text{LCT}}(\psi) \right] \psi \\ &\quad + \hat{U}_{\hat{V}_{\text{tot}}}(\Delta t)^{-1}\hat{1} \\ &= \hat{U}_{\hat{V}_{\text{tot}}}(\Delta t)^{-1} \left[\hat{1} + \frac{i}{\hbar} \Delta t \hat{V}_{\text{LCT}}(\psi) \right], \end{aligned} \quad (18)$$

where we employed, in the third line, the generalized complex derivative⁶⁵ of the nonlinear potential, which is given by the bra vector

$$\frac{\delta}{\delta\psi} \hat{V}_{\text{LCT}}(\psi) = -\hat{\mu} \cdot \frac{\delta}{\delta\psi} \vec{E}_{\text{LCT}}(\psi) = \mp \lambda i \hat{\mu} \cdot \langle \psi | [\hat{\mu}, \hat{O}]. \quad (19)$$

IV. NUMERICAL EXAMPLES

Integrators presented in Sec. III were tested on a local control simulation in a two-dimensional model describing the *cis-trans* photo-isomerization of retinal. This ultrafast reaction, which is mediated by a conical intersection, is the first event occurring in the biological process of vision. The model, which uses the reaction coordinate θ , an angle describing the torsional motion of the retinal molecule, and a vibronically active coupling mode q_c , was taken from Ref. 66 and we used it as described in Ref. 35 (see Fig. S3 of the supplementary material of Ref. 35 for the two diabatic potential energy surfaces of the model). We used the same grid [a regular direct-product grid consisting of 128 points between $\theta = \pm\pi/2$ a.u. and 64 points between $q_c = \pm 9$ a.u.], the same initial state [a two-dimensional Gaussian wavepacket $\psi_0(x) = \prod_{j=1}^2 (\sigma_{0,j}^2 \pi)^{-1/4} \exp[ip_{0,j}(x_j - q_{0,j})/\hbar - (x_j - q_{0,j})^2/2\sigma_{0,j}^2]$, with $x := (\theta, q_c)$, initial positions and momentum $q_0 = p_0 = (0, 0)$ a.u. and initial width $\sigma_0 = (0.128, 1)$ a.u., corresponding to the ground vibrational state of the harmonic fit of the ground electronic potential energy surface], and the same initial populations $P_1(0) = 0.999$ and $P_2 = 0.001$ of the

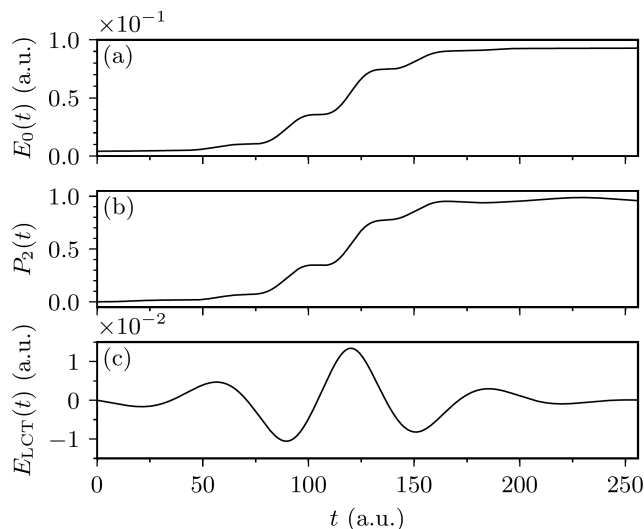


FIG. 1. Local control simulation whose goal is increasing the molecular energy $E_0(t)$. (a) Molecular energy. (b) Excited state population. (c) Pulse obtained by LCT.

ground and excited electronic states, respectively. The kinetic and potential propagations were performed using the dynamic Fourier method^{29–32} with the Fastest Fourier Transform in the West 3 (FFTW3) library⁶⁷ to change between position and momentum representations. Following Ref. 35, we assumed that the electric dipole moment operator $\hat{\mu}$ was coordinate independent (Condon approximation) and aligned with the electric field \vec{E}_{LCT} . Consequently, we could drop the vector symbols in Eq. (5), i.e., replace the vectors $\hat{\mu}$ and \vec{E}_{LCT} with the scalars $\hat{\mu}$ and E_{LCT} . In all simulations, the electric dipole moment operator had unit transition (offdiagonal) elements ($\hat{\mu}_{12} = \hat{\mu}_{21} = 1$ a.u.) and zero diagonal elements ($\hat{\mu}_{11} = \hat{\mu}_{22} = 0$ a.u.); which allowed the control field to couple the two electronic states and simultaneously avoid coupling between the vibrational states. Throughout this section, the **bold** font denotes electronic operators expressed as $S \times S$ matrices in the basis of S electronic states and that the hat $\hat{\cdot}$ denotes nuclear operators acting on the Hilbert space of nuclear wavefunctions, i.e., square-integrable functions of D continuous degrees of freedom.

In all simulations, we used LCT for increasing the molecular energy $E_0(t) := \langle \hat{\mathbf{H}}_0 \rangle_{\psi_t}$ of the system, which required employing the molecular energy operator $\hat{\mathbf{H}}_0$ as the target observable. First, we performed the local control by solving the NL-TDSE (1) up to the final time $t_f = 256$ a.u. using the implicit TVT split-operator algorithm and intensity parameter $\lambda = 1.534 \times 10^{-1}$, which was chosen arbitrarily so that the amplitude of the obtained control field was not too high and, at the same time, strong enough to induce a significant increase of molecular energy (see Fig. 1). The results indicate a successful increase in molecular energy [panel (a)] and, as

predicted in Sec. II, this increase is monotonic because the molecular energy operator commutes with itself. Indeed, by construction, there are no nonzero diagonal elements in the electric dipole moment operator and, as a result, vibrational energy cannot be added by the control pulse ($\langle [\hat{\mu}, \hat{\mathbf{T}}] \rangle_{\psi_t} = 0$). Instead, due to the presence of nonzero transition (offdiagonal) elements in the electric dipole moment, the control pulse increases the electronic energy of our system by increasing the excited state population $P_2(t)$ [panel (b)]; this is confirmed by the carrier frequency of the control pulse [panel (c)], which corresponds to an electronic transition between the two states.

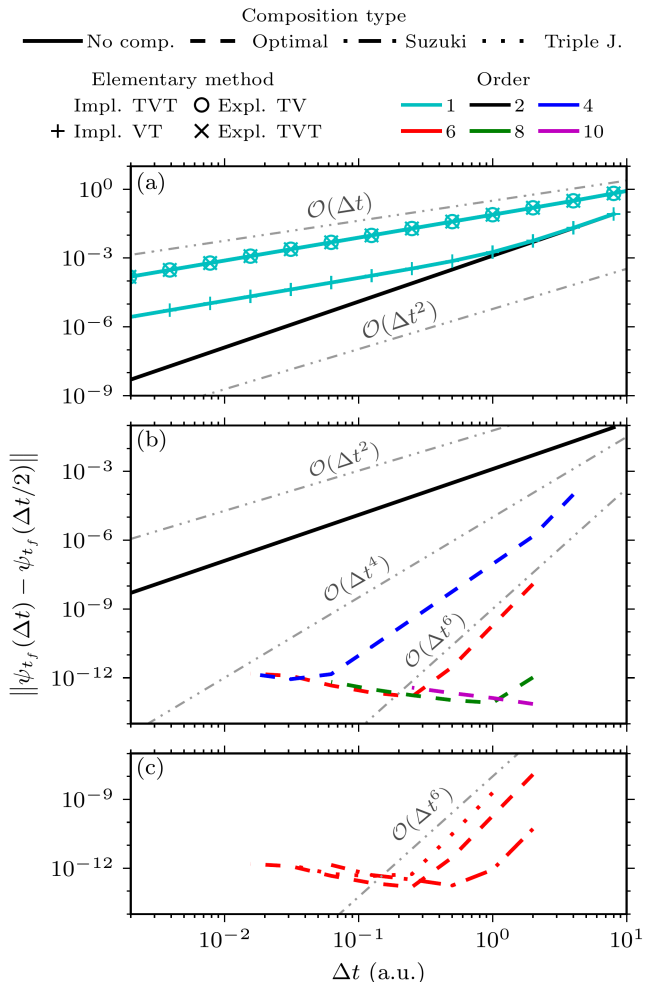


FIG. 2. Convergence of the molecular wavefunction at the final time $t_f = 256$ a.u. achieved by the local energy control. (a) First-order and implicit TVT methods. (b) Methods obtained with the optimal composition (Suzuki's fractal is the optimal fourth-order composition scheme⁵⁷). (c) Sixth-order methods obtained with different composition schemes.

To verify the order of convergence of the integrators presented in Sec. III, the same simulation was repeated for each integrator with different time steps, and the errors in the obtained wavefunctions were compared at the final time $t_f = 256$ a.u. To measure the convergence er-

ror, we used the L_2 -norm $\|\psi_{t_f}(\Delta t) - \psi_{t_f}(\Delta t/2)\|$ where $\psi_t(\Delta t)$ denotes the wavefunction at time t obtained using a time step Δt . Figure 2 shows the convergence behavior of various integrators, including higher-order integrators obtained by composing the implicit TVT method with the triple-jump, Suzuki's fractal, and optimal composition schemes. The results in panel (a) indicate that the implicit TVT method has the expected order of convergence and that it is, for a given time step, more accurate than all first-order methods, including the approximate explicit TVT algorithm. Comparison between different orders of the optimal composition of the implicit TVT algorithm [panel (b)] shows that, for a given time step, a higher order of composition yields more accurate integrators. Similarly, comparing sixth-order methods obtained with different composition schemes [panel (c)] indicates that, for a given time step, Suzuki's fractal composition is more accurate than both the optimal and triple-jump compositions. Note that after reaching a machine precision plateau, the higher-order integrators show a slight increase in the error with a decreasing time step, which is due to the accumulation of roundoff errors since the number of steps increases for a fixed total time of simulation. Moreover, some results for high-order integrators could not be obtained because they did not converge at large time steps (the difference between the initial guess and the implicit solution was too large for the Newton-Raphson method to converge) and became computationally unaffordable at smaller time steps, when the Newton-Raphson method was converging.

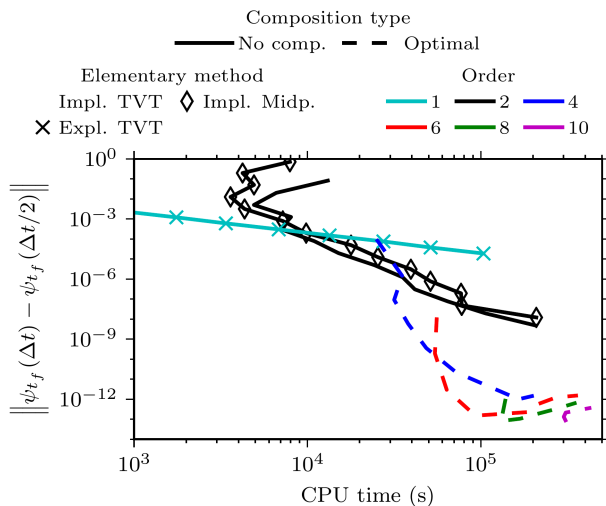


FIG. 3. Efficiency of various integrators used for simulating the local energy control of retinal up to the final time $t_f = 256$ a.u.

The higher-order integrators, obtained by composition, require performing many substeps at each time step, which increases their cost. To check that greater accuracy for a given time step is not detrimental to efficiency, in Fig. 3 we plot the dependence of errors of the

wavefunctions obtained by various methods on the computational cost, measured by the central processing unit (CPU) time (see also Fig. S2 of the supplementary material, which displays the efficiency results for all studied methods).

Figure 3 demonstrates that, if high accuracy is desired, the higher-order integrators are more efficient even though they require performing many substeps at each time step. For example, below an error of 3×10^{-4} , the second-order implicit TVT split-operator algorithm is already more efficient than the approximate explicit TVT split-operator algorithm. Figure 3 also shows that the implicit TVT split-operator algorithm is more efficient than the implicit midpoint method, indicating that the implicit split-operator algorithm is the method of choice for separable Hamiltonians and that the implicit midpoint method should only be used when the Hamiltonian is not separable. Indeed, for errors below 7×10^{-4} , the TVT split-operator algorithm is more efficient than the implicit midpoint method.

In Fig. 4, we checked the preservation of geometric properties by the implicit and approximate explicit TVT methods (see Fig. S3 of the supplementary material for a version of this figure which displays the results for all the elementary methods). Since geometric integrators preserve geometric properties exactly regardless of the size of the time step, we intentionally used a rather large time step $\Delta t = 2^{-2}$ a.u. We also extended the final time of the simulation to $t_f = 2048$ a.u. in order to induce more dynamics. Following Ref. 35, we modified the grid to 256 points between $\theta = \pm 3\pi/2$ a.u. and 64 points between $q_c = \pm 9$ a.u. to ensure that the grid representation of the wavefunction at the new final time t_f remains converged. The results show that while both the implicit and approximate explicit TVT integrators conserve the norm [panel (a)], only the implicit TVT method is time-reversible [panel (b)]. However, due to the nonlinearity of the time-dependent Schrödinger equation and the accumulation of roundoff errors, one observes a gradual loss of time reversibility as the time increases. (See Sec. V of the supplementary material of Ref. 35 for a detailed analysis of this loss of time-reversibility.) The bottom three panels of Fig. 4 (and Fig. S3) demonstrate that none of the methods conserves the inner product [panel (c)], distance between two states [panel (d)], or total energy [panel (e)], because these properties are not conserved even by the exact nonlinear evolution operator (4).

Figure 5 analyze the norm conservation [panel (a)] and time reversibility [panel (b)] of various integrators at the final time $t_f = 256$ a.u. as a function of the time step (see Fig. S4 of the supplementary material for a version of this figure with all the studied methods). As expected, all the integrators presented in Sec. III conserve the norm, regardless of the time step. Whereas the first-order integrators are irreversible (the time reversibility is satisfied only to the first order in the time step), the implicit midpoint, TVT and TVT methods as well as compositions of the latter are time-reversible for all time steps (see

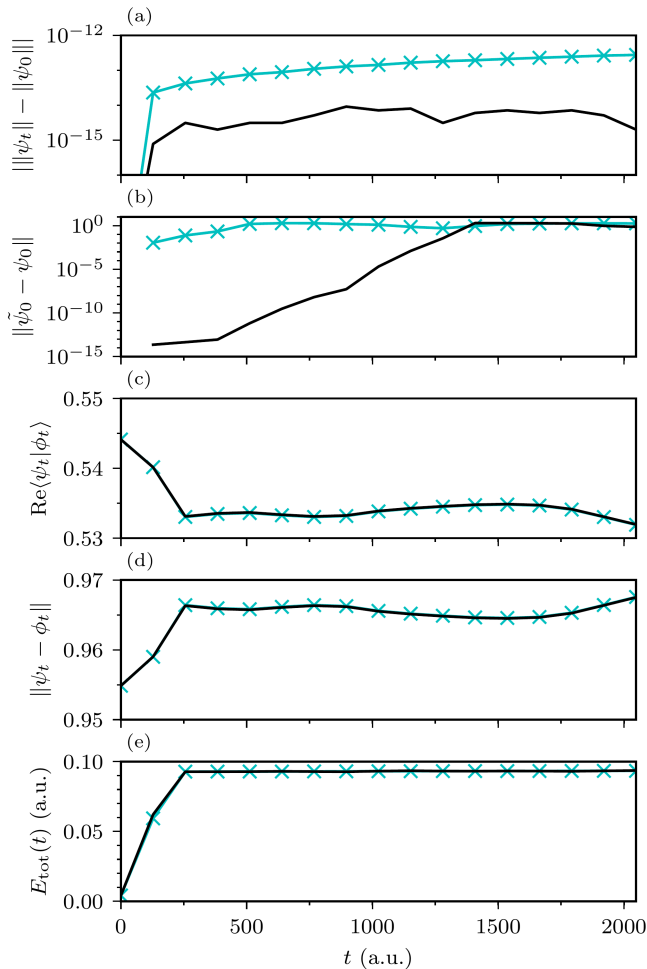


FIG. 4. Time dependence of the geometric properties of the implicit and approximate explicit TVT methods used for simulating the local energy control up to the final time $t_f = 2048$ a.u. (a) Norm of the wavefunction. (b) Time reversibility. (c) Inner product. (d) Distance between two states (conservation of this distance would imply stability). (e) Total energy $E_{\text{tot}}(t) := E_0(t) + \langle \hat{\mathbf{V}}_{\text{LCT}}(\psi_t) \rangle_{\psi_t}$. Time reversibility is measured by the distance between the initial state ψ_0 and a “forward-backward” propagated state $\tilde{\psi}_0 := \hat{U}(0, t; \psi) \hat{U}(t, 0; \psi) \psi_0$, where $\hat{U}(0, t; \psi)$ denotes a nonlinear evolution operator with a reversed time flow [see Eq. (A6)]. The state ϕ_0 is ψ_0 displaced along the reaction coordinate [a two-dimensional Gaussian wavepacket with parameters $q_0 = (0.1, 0)$, $p_0 = (0, 0)$, and $\sigma_0 = (0.128, 0)$ a.u.]. Line labels are the same as in Fig. 2.

Fig. S4).

V. CONCLUSION

We presented high-order integrators for solving the NL-TDSE with separable Hamiltonians. In contrast to their first-order explicit versions, the proposed methods, obtained by composing an implicit split-operator algo-

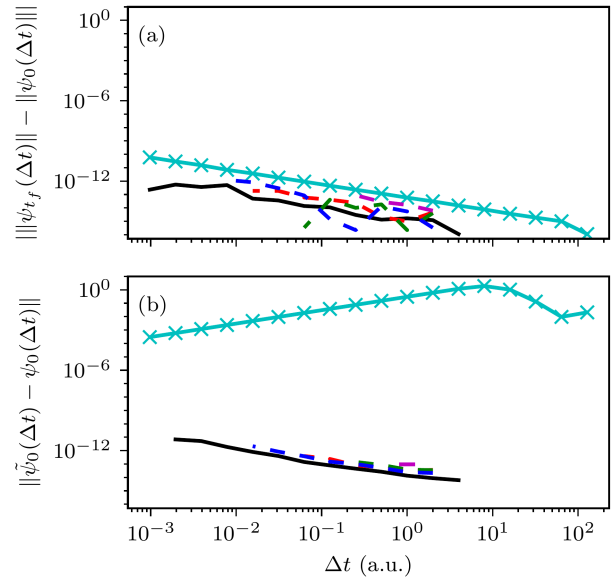


FIG. 5. Norm conservation (a) and time reversibility (b) of various integrators at the final time $t_f = 256$ a.u. as a function of the time step Δt used for the local energy control of retinal. Reversibility is measured as in Fig. 4 and line labels are the same as in Fig. 2.

rithm, preserve all geometric properties of the exact solution: they are symmetric, time-reversible, and norm-conserving. Moreover, the proposed integrators are more efficient than both the explicit split-operator algorithm and the recently proposed³⁵ compositions of the implicit midpoint method.

SUPPLEMENTARY MATERIAL

The supplementary material contains analogues of Figs. 2–5 of the main text that display the numerical results for all studied methods.

ACKNOWLEDGMENTS

The authors thank Seonghoon Choi for useful discussions and acknowledge the financial support from the Swiss National Science Foundation within the National Center of Competence in Research “Molecular Ultrafast Science and Technology” (MUST) and from the European Research Council (ERC) under the European Union’s Horizon 2020 research and innovation program (grant agreement No. 683069 – MOLECULE).

AUTHOR DECLARATIONS

Conflict of interest

The authors have no conflicts to disclose.

DATA AVAILABILITY

The data that support the findings of this study are openly available in Zenodo at <http://doi.org/10.5281/zenodo.5566833>.

Appendix A: Geometric properties of various integrators

Here we demonstrate the geometric properties of the explicit TV and implicit VT, TVT, and VTV algorithms. We refer the reader to the Appendix of Ref. 35 for the analogous proofs for the approximate explicit TVT algorithm and the implicit midpoint method.

1. Norm conservation

The evolution operator $\hat{U}_{\hat{T}}(\Delta t)$ of the Hermitian kinetic energy operator \hat{T} conserves the norm $\|\psi_t\|$ of the state ψ_t because

$$\begin{aligned} \|\hat{U}_{\hat{T}}(\Delta t)\psi_t\|^2 &= \langle \psi_t | \hat{U}_{\hat{T}}(\Delta t)^\dagger \hat{U}_{\hat{T}}(\Delta t) \psi_t \rangle = \langle \psi_t | \psi_t \rangle \\ &= \|\psi_t\|^2, \end{aligned} \quad (\text{A1})$$

where we used the relation

$$\hat{U}_{\hat{A}}(\Delta t)^\dagger = (e^{-i\hat{A}\Delta t/\hbar})^\dagger = \hat{U}_{\hat{A}}(\Delta t)^{-1}, \quad (\text{A2})$$

which holds for any Hermitian operator \hat{A} , to obtain the second equality.

For the potential evolution operator, we first assume that while the operator $\hat{V}_{\text{tot}} : \psi \mapsto \hat{V}_{\text{tot}}(\psi)\psi$ is nonlinear, for each ϕ the operator $\hat{V}_{\text{tot}}(\phi) : \psi \mapsto \hat{V}_{\text{tot}}(\phi)\psi$ is linear. Moreover, we assume that $\hat{V}_{\text{tot}}(\phi)$ has real expectation values $\langle \hat{V}_{\text{tot}}(\phi) \rangle_\psi$ in any state ψ , which for a linear operator implies that it is Hermitian. Therefore, the evolution operator $\hat{U}_{\hat{V}_{\text{tot}}(\phi)}(\Delta t)$ conserves, for any ϕ , the norm of the state ψ_t because

$$\begin{aligned} \|\hat{U}_{\hat{V}_{\text{tot}}(\phi)}(\Delta t)\psi_t\|^2 &= \langle \psi_t | \hat{U}_{\hat{V}_{\text{tot}}(\phi)}(\Delta t)^\dagger \hat{U}_{\hat{V}_{\text{tot}}(\phi)}(\Delta t) \psi_t \rangle \\ &= \langle \psi_t | \psi_t \rangle = \|\psi_t\|^2, \end{aligned} \quad (\text{A3})$$

where we used Eq. (A2) to obtain the second equality.

Composing two norm-conserving evolution operators $\hat{U}_{\hat{A}}$ and $\hat{U}_{\hat{B}}$ of Hermitian operators \hat{A} and \hat{B} , respectively, yields a norm-conserving integrator $\hat{U}_{\hat{A}\hat{B}}(\Delta t) := \hat{U}_{\hat{A}}(\Delta t)\hat{U}_{\hat{B}}(\Delta t)$. Indeed, we have

$$\begin{aligned} \|\hat{U}_{\hat{A}\hat{B}}(\Delta t)\psi_t\|^2 &= \|\hat{U}_{\hat{A}}(\Delta t)\psi_t'\|^2 = \|\psi_t'\|^2 \\ &= \|\hat{U}_{\hat{B}}(\Delta t)\psi_t\|^2 = \|\psi_t\|^2, \end{aligned} \quad (\text{A4})$$

where $\psi_t' := \hat{U}_{\hat{B}}(\Delta t)\psi_t$. Therefore, all proposed integrators (including the integrators obtained by symmetric composition of TVT or VTV algorithms) conserve the norm because they are all compositions of the norm-conserving integrators $\hat{U}_{\hat{T}}(\Delta t)$ and $\hat{U}_{\hat{V}_{\text{tot}}(\phi)}(\Delta t)$.

2. Symmetry and time-reversibility

In the theory of dynamical systems, an *adjoint* $\hat{U}_{\text{appr}}(\psi)^*$ of $\hat{U}_{\text{appr}}(\psi)$ is defined as the inverse of the evolution operator taken with a reversed time flow:

$$\hat{U}_{\text{appr}}(t + \Delta t, t; \psi)^* := \hat{U}_{\text{appr}}(t, t + \Delta t; \psi)^{-1}. \quad (\text{A5})$$

If the evolution operator is equal to its adjoint, i.e., if $\hat{U}(t, t_0; \psi) = \hat{U}(t, t_0; \psi)^*$, the evolution operator $\hat{U}(t, t_0; \psi)$ is said to be symmetric. Time reversibility results from symmetry because for a symmetric evolution operator, propagating an initial state ψ_{t_0} forward to time t and then backward to time t_0 , recovers ψ_{t_0} , i.e.,

$$\begin{aligned} \hat{U}_{\text{appr}}(t_0, t; \psi) \hat{U}_{\text{appr}}(t, t_0; \psi) \psi_{t_0} \\ &= \hat{U}_{\text{appr}}(t_0, t; \psi)^* \hat{U}_{\text{appr}}(t, t_0; \psi) \psi_{t_0} \\ &= \hat{U}_{\text{appr}}(t, t_0; \psi)^{-1} \hat{U}_{\text{appr}}(t, t_0; \psi) \psi_{t_0} = \psi_{t_0}. \end{aligned} \quad (\text{A6})$$

Neither the explicit TV nor implicit VT method is symmetric because

$$\begin{aligned} \hat{U}_{TV}(t + \Delta t, t; \psi_t)^* &= \hat{U}_{TV}(t, t + \Delta t; \psi_{t+\Delta t})^{-1} \\ &= [\hat{U}_{\hat{T}}(-\Delta t) \hat{U}_{\hat{V}_{\text{tot}}(\psi_{t+\Delta t})}(-\Delta t)]^{-1} \\ &= \hat{U}_{\hat{V}_{\text{tot}}(\psi_{t+\Delta t})}(\Delta t) \hat{U}_{\hat{T}}(\Delta t) \\ &= \hat{U}_{VT}(t + \Delta t, t; \psi_{t+\Delta t}) \\ &\neq \hat{U}_{TV}(t + \Delta t, t; \psi_t) \end{aligned} \quad (\text{A7})$$

and

$$\begin{aligned} \hat{U}_{VT}(t + \Delta t, t; \psi_{t+\Delta t})^* &= \hat{U}_{VT}(t, t + \Delta t; \psi_t)^{-1} \\ &= [\hat{U}_{\hat{V}_{\text{tot}}(\psi_t)}(-\Delta t) \hat{U}_{\hat{T}}(-\Delta t)]^{-1} \\ &= \hat{U}_{\hat{T}}(\Delta t) \hat{U}_{\hat{V}_{\text{tot}}(\psi_t)}(\Delta t) \\ &= \hat{U}_{TV}(t + \Delta t, t; \psi_t) \\ &\neq \hat{U}_{VT}(t + \Delta t, t; \psi_{t+\Delta t}). \end{aligned} \quad (\text{A8})$$

As a result, neither the TV nor VT method is time-reversible.

From Eqs. (A7) and (A8), we notice that the explicit TV and VT methods are, in fact, adjoints of each other, i.e., $\hat{U}_{TV}^* = \hat{U}_{VT}$ and $\hat{U}_{VT}^* = \hat{U}_{TV}$. In general, the composition of adjoint methods \hat{U} and \hat{U}^* , each with a time step $\Delta t/2$, yields symmetric methods $\hat{U}\hat{U}^*$ and $\hat{U}^*\hat{U}$.⁵⁰ Because the implicit TVT and VTV methods are such compositions of adjoint TV and VT methods, both TVT and VTV integrators are symmetric. Applying symmetric composition schemes to these symmetric methods

will always yield a symmetric method.⁵⁰ Therefore, the proposed high-order integrators are also symmetric and time-reversible.

- ¹P. A. M. Dirac, *Math. Proc. Camb. Phil. Soc.* **26**, 376 (1930).
- ²J. Frenkel, *Wave mechanics* (Clarendon Press, Oxford, 1934).
- ³J. Broeckhove, L. Lathouwers, E. Kesteloot, and P. V. Leuven, *Chem. Phys. Lett.* **149**, 547 (1988).
- ⁴C. Lubich, *From Quantum to Classical Molecular Dynamics: Reduced Models and Numerical Analysis*, 12th ed. (European Mathematical Society, Zürich, 2008).
- ⁵H.-D. Meyer, U. Manthe, and L. S. Cederbaum, *Chem. Phys. Lett.* **165**, 73 (1990).
- ⁶U. Manthe, H.-D. Meyer, and L. S. Cederbaum, *J. Chem. Phys.* **97**, 3199 (1992).
- ⁷M. Beck, A. Jäckle, G. Worth, and H.-D. Meyer, *Phys. Rep.* **324**, 1 (2000).
- ⁸R. D. Coalson and M. Karplus, *J. Chem. Phys.* **93**, 3919 (1990).
- ⁹C. Lasser and C. Lubich, *Acta Numerica* **29**, 229 (2020).
- ¹⁰I. Burghardt, K. Giri, and G. A. Worth, *J. Chem. Phys.* **129**, 174104 (2008).
- ¹¹G. W. Richings, I. Polyak, K. E. Spinlove, G. A. Worth, I. Burghardt, and B. Lasorne, *Int. Rev. Phys. Chem.* **34**, 269 (2015).
- ¹²E. J. Heller, *J. Chem. Phys.* **62**, 1544 (1975).
- ¹³A. Patoz, T. Begušić, and J. Vaníček, *J. Phys. Chem. Lett.* **9**, 2367 (2018).
- ¹⁴T. Begušić and J. Vaníček, *J. Chem. Phys.* **153**, 024105 (2020).
- ¹⁵G. A. Hagedorn, *Commun. Math. Phys.* **71**, 77 (1980).
- ¹⁶E. Faou, V. Gradinaru, and C. Lubich, *SIAM J. Sci. Comp.* **31**, 3027 (2009).
- ¹⁷T. Begušić, M. Cordova, and J. Vaníček, *J. Chem. Phys.* **150**, 154117 (2019).
- ¹⁸A. Prlj, T. Begušić, Z. T. Zhang, G. C. Fish, M. Wehrle, T. Zimmermann, S. Choi, J. Roulet, J.-E. Moser, and J. Vaníček, *J. Chem. Theory Comput.* **16**, 2617 (2020).
- ¹⁹C. Lanczos, *J. Res. Nat. Bur. Stand.* **45**, 255 (1950).
- ²⁰C. Leforestier, R. H. Bisseling, C. Cerjan, M. D. Feit, R. Friesner, A. Guldberg, A. Hammerich, G. Jolicard, W. Karlein, H.-D. Meyer, N. Lipkin, O. Roncero, and R. Kosloff, *J. Comp. Phys.* **94**, 59 (1991).
- ²¹T. J. Park and J. C. Light, *J. Chem. Phys.* **85**, 5870 (1986).
- ²²E. P. Gross, *Il Nuovo Cimento* (1955-1965) **20**, 454 (1961).
- ²³L. P. Pitaevskii, *Sov. Phys. JETP* **13**, 451 (1961).
- ²⁴R. Carles, *Ann. Henri Poincaré* **3**, 757 (2002).
- ²⁵R. Carles, P. A. Markowich, and C. Sparber, *Nonlinearity* **21**, 2569 (2008).
- ²⁶A. Minguzzi, S. Succi, F. Toschi, M. Tosi, and P. Vignolo, *Phys. Rep.* **395**, 223 (2004).
- ²⁷M. H. Anderson, J. R. Ensher, M. R. Matthews, C. E. Wieman, and E. A. Cornell, *Science* **269**, 198 (1995).
- ²⁸F. Dalfovo, S. Giorgini, L. P. Pitaevskii, and S. Stringari, *Rev. Mod. Phys.* **71**, 463 (1999).
- ²⁹M. D. Feit, J. A. Fleck, Jr., and A. Steiger, *J. Comp. Phys.* **47**, 412 (1982).
- ³⁰D. Kosloff and R. Kosloff, *J. Comp. Phys.* **52**, 35 (1983).
- ³¹R. Kosloff and D. Kosloff, *J. Chem. Phys.* **79**, 1823 (1983).
- ³²D. J. Tannor, *Introduction to Quantum Mechanics: A Time-Dependent Perspective* (University Science Books, Sausalito, 2007).
- ³³W. Bao, D. Jaksch, and P. A. Markowich, *J. Comp. Phys.* **187**, 318 (2003).
- ³⁴J. Roulet, S. Choi, and J. Vaníček, *J. Chem. Phys.* **150**, 204113 (2019).
- ³⁵J. Roulet and J. Vaníček, *J. Chem. Phys.* **154**, 154106 (2021).
- ³⁶R. Kosloff, S. A. Rice, P. Gaspard, S. Tersigni, and D. J. Tannor, *Chem. Phys.* **139**, 201 (1989).
- ³⁷R. Kosloff, A. D. Hammerich, and D. Tannor, *Phys. Rev. Lett.* **69**, 2172 (1992).
- ³⁸Y. Ohtsuki, H. Kono, and Y. Fujimura, *J. Chem. Phys.* **109**, 9318 (1998).
- ³⁹M. Yamaki, K. Hoki, Y. Ohtsuki, H. Kono, and Y. Fujimura, *J. Am. Chem. Soc.* **127**, 7300 (2005).
- ⁴⁰P. Marquetand, S. Gräfe, D. Scheidel, and V. Engel, *J. Chem. Phys.* **124**, 054325 (2006).
- ⁴¹P. Marquetand and V. Engel, *Chem. Phys. Lett.* **426**, 263 (2006).
- ⁴²P. Marquetand and V. Engel, *J. Chem. Phys.* **127**, 084115 (2007).
- ⁴³V. Engel, C. Meier, and D. J. Tannor, *Adv. Chem. Phys.* **141**, 29 (2009).
- ⁴⁴L. Bomble, A. Chenel, C. Meier, and M. Desouter-Lecomte, *J. Chem. Phys.* **134**, 204112 (2011).
- ⁴⁵S. Vranckx, J. Loreau, N. Vaeck, C. Meier, and M. Desouter-Lecomte, *J. Chem. Phys.* **143**, 164309 (2015).
- ⁴⁶P. Vindel-Zandbergen, C. Meier, and I. R. Sola, *Chem. Phys.* **478**, 97 (2016).
- ⁴⁷R. De Vogelaere, “Methods of integration which preserve the contact transformation property of the hamilton equations,” (1956), Report No. 4, Department of Mathematics, University of Notre Dame.
- ⁴⁸E. Hairer, C. Lubich, and G. Wanner, *Acta Numerica* **12**, 399 (2003).
- ⁴⁹B. Leimkuhler and S. Reich, *Simulating Hamiltonian Dynamics* (Cambridge University Press, 2004).
- ⁵⁰E. Hairer, C. Lubich, and G. Wanner, *Geometric Numerical Integration: Structure-Preserving Algorithms for Ordinary Differential Equations* (Springer Berlin Heidelberg New York, 2006).
- ⁵¹H. Yoshida, *Phys. Lett. A* **150**, 262 (1990).
- ⁵²M. Suzuki, *Phys. Lett. A* **146**, 319 (1990).
- ⁵³W. Kohan and R.-C. Li, *Math. Comput.* **66**, 1089 (1997).
- ⁵⁴M. Sofroniou and G. Spaletta, *Optim. Method Softw.* **20**, 597 (2005).
- ⁵⁵G. C. Schatz and M. A. Ratner, *Quantum Mechanics in Chemistry* (Dover Publications, 2002).
- ⁵⁶M. Abe, T. Kawakami, S. Ohata, K. Nozaki, and M. Nojima, *J. Am. Chem. Soc.* **126**, 2838 (2004).
- ⁵⁷S. Choi and J. Vaníček, *J. Chem. Phys.* **150**, 204112 (2019).
- ⁵⁸C. Lubich, *Math. Comput.* **77**, 2141 (2008).
- ⁵⁹M. Thalhammer, *SIAM J. Num. Analysis* **50**, 3231 (2012).
- ⁶⁰Y. Saad and M. H. Schultz, *SIAM J. Sci. Comp.* **7**, 856 (1986).
- ⁶¹W. H. Press, S. A. Teukolsky, W. T. Vetterling, and B. P. Flannery, *Numerical recipes in C* (Cambridge University Press, Cambridge, UK, 1992).
- ⁶²Y. Saad, *Iterative Methods for Sparse Linear Systems*, 2nd ed. (SIAM, 2003).
- ⁶³W. E. Arnoldi, *Quart. Appl. Math* **9**, 17 (1951).
- ⁶⁴Y. Saad, *Linear Algebra Appl.* **34**, 269 (1980).
- ⁶⁵K. B. Petersen and M. S. Pedersen, “The matrix cookbook,” (2012).
- ⁶⁶S. Hahn and G. Stock, *J. Phys. Chem. B* **104**, 1146 (2000).
- ⁶⁷M. Frigo and S. G. Johnson, *Proc. IEEE* **93**, 216 (2005).

Supplementary material: An implicit split-operator algorithm for the nonlinear time-dependent Schrödinger equation

Julien Roulet^{a)} and Jiří Vaníček^{b)}

Laboratory of theoretical physical chemistry, Institut des sciences et ingénieries Chimiques, Ecole Polytechnique Fédérale de Lausanne (EPFL), Lausanne, Switzerland

(Dated: 12 November 2021)

^{a)}Electronic mail: julien.roulet@epfl.ch

^{b)}Electronic mail: jiri.vanicek@epfl.ch

SI. RESULTS FOR ALL STUDIED METHODS

To avoid clutter in the figures of the main text, we showed there only the results of some studied methods. Here, we show the results displayed in Figs. 2–5 of the main text for all the studied methods. Note that the results of some high-order methods could not be obtained because they did not converge at large time steps (the difference between the initial guess and the implicit solution was too large for the Newton-Raphson method to converge) and became computationally unaffordable at smaller time steps, when the Newton-Raphson method was converging.

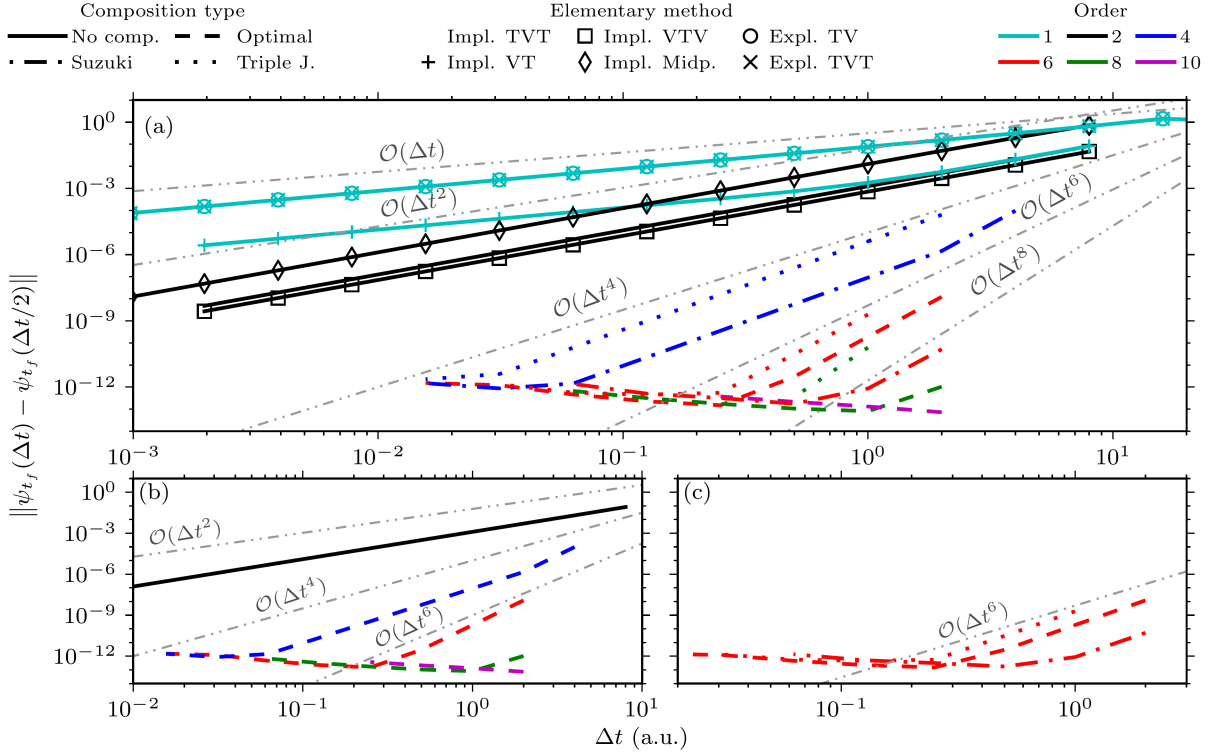


FIG. S1. Convergence of the molecular wavefunction at the final time $t_f = 256$ a.u. achieved by the local energy control. (a) All studied methods, including symmetric compositions of the TVT split-operator algorithm. (b) Methods obtained with the optimal composition (Suzuki's fractal is the optimal fourth-order composition scheme). (c) Sixth-order methods obtained with different composition schemes.

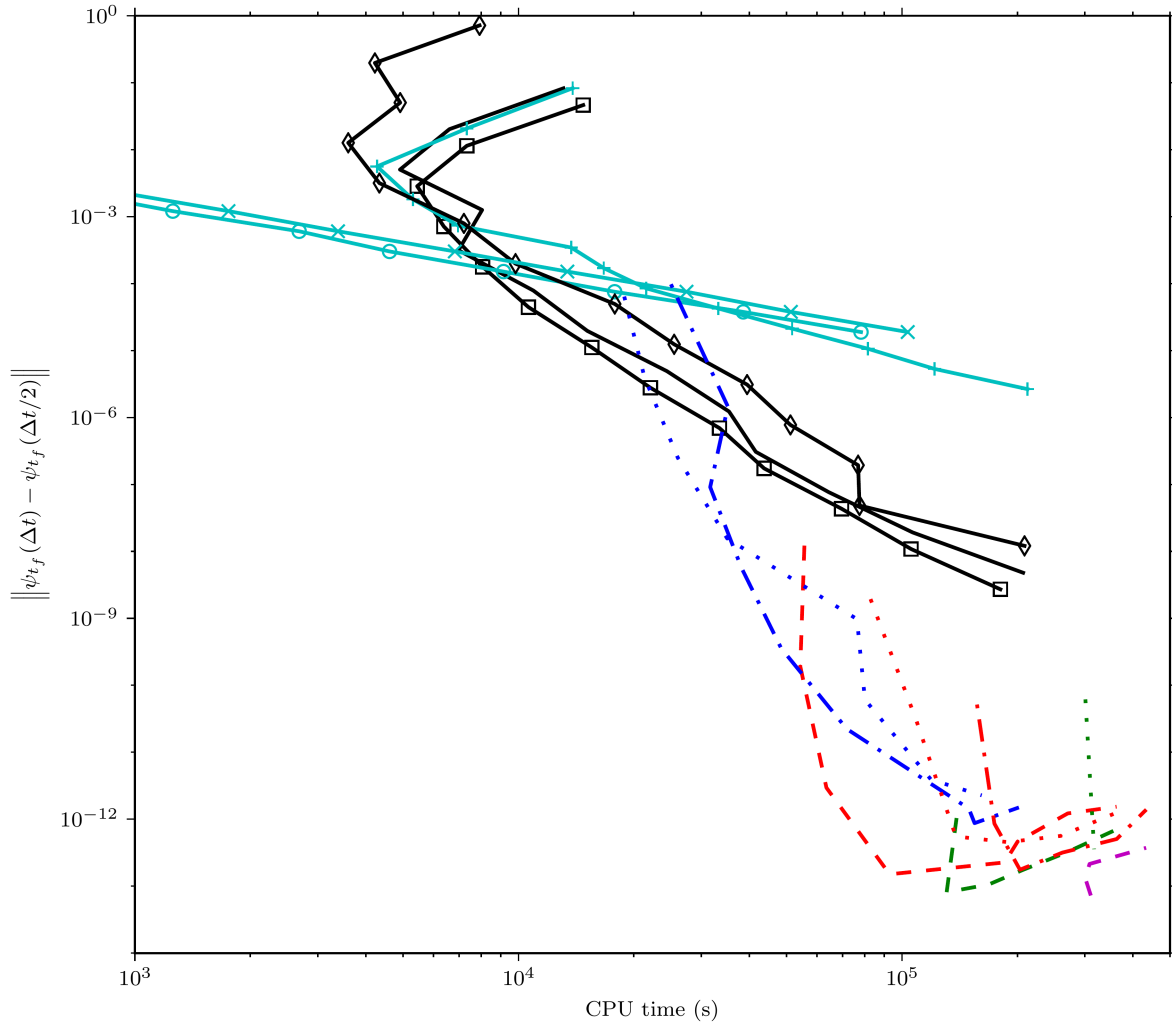


FIG. S2. Efficiency of the integrators used for simulating the local energy control of retinal up to the final time $t_f = 256$ a.u. Line labels are the same as in Fig. S1.

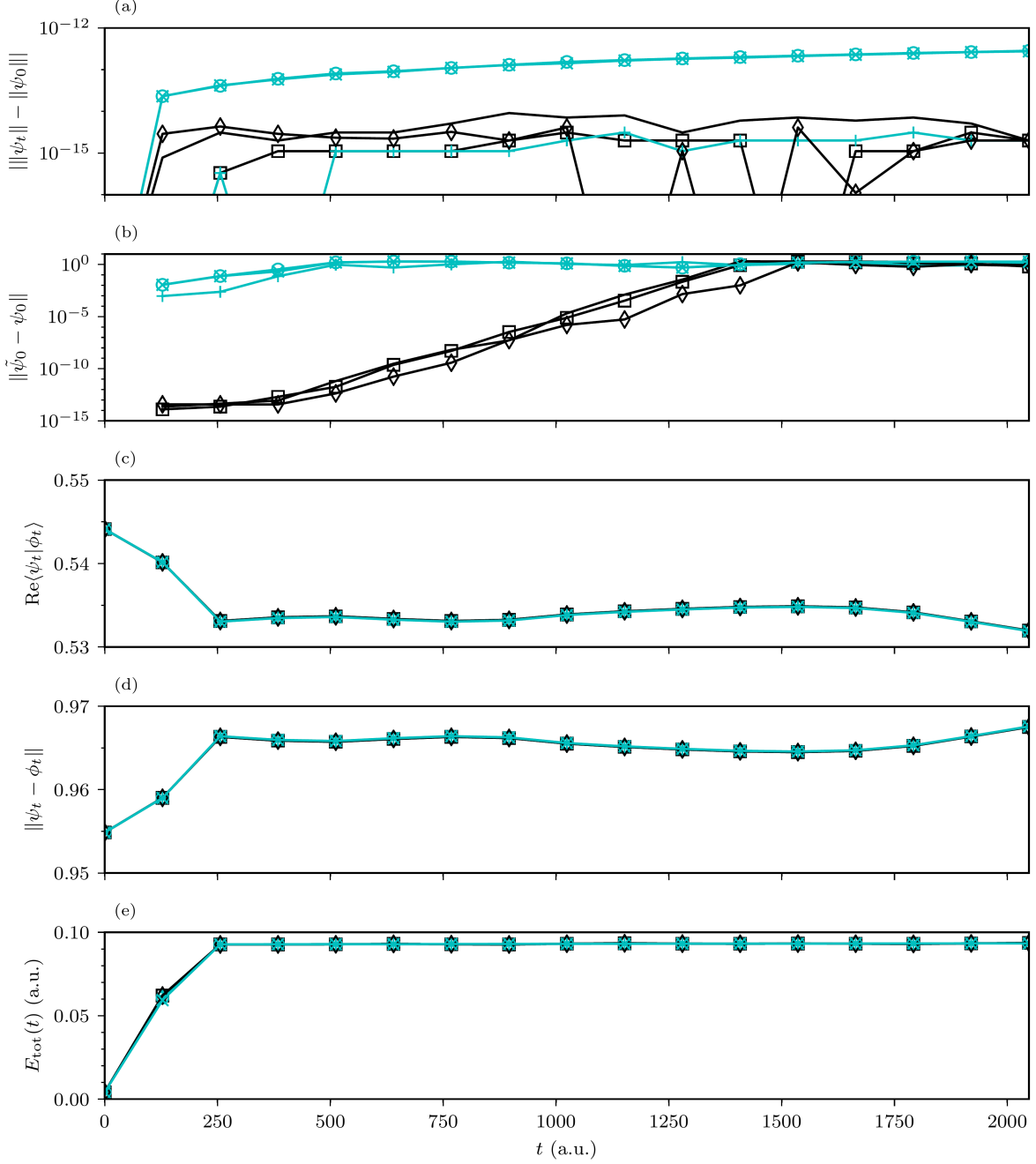


FIG. S3. Time dependence of the geometric properties of the elementary integrators used for simulating the local energy control up to the final time $t_f = 2048$ a.u. (a) Norm of the wavefunction. (b) Time reversibility. (c) Inner product. (d) Distance between two states (which would imply stability). (e) Total energy $E_{\text{tot}}(t) := E_0(t) + \langle \hat{\mathbf{V}}_{\text{LCT}}(\psi_t) \rangle_{\psi_t}$. Time reversibility is measured by the distance between the initial state ψ_0 and a “forward-backward” propagated state $\tilde{\psi}_0 := \hat{U}(0, t; \psi) \hat{U}(t, 0; \psi) \psi_0$, where $\hat{U}(0, t; \psi)$ denotes a nonlinear evolution operator with a reversed time flow [see Eq. (A6)]. The state ϕ_0 is ψ_0 displaced along the reaction coordinate [a two-dimensional Gaussian wavepacket with parameters $q_0 = (0.1, 0)$, $p_0 = (0, 0)$, and $\sigma_0 = (0.128, 0)$ a.u.]. Line labels are the same as in Fig. S1.

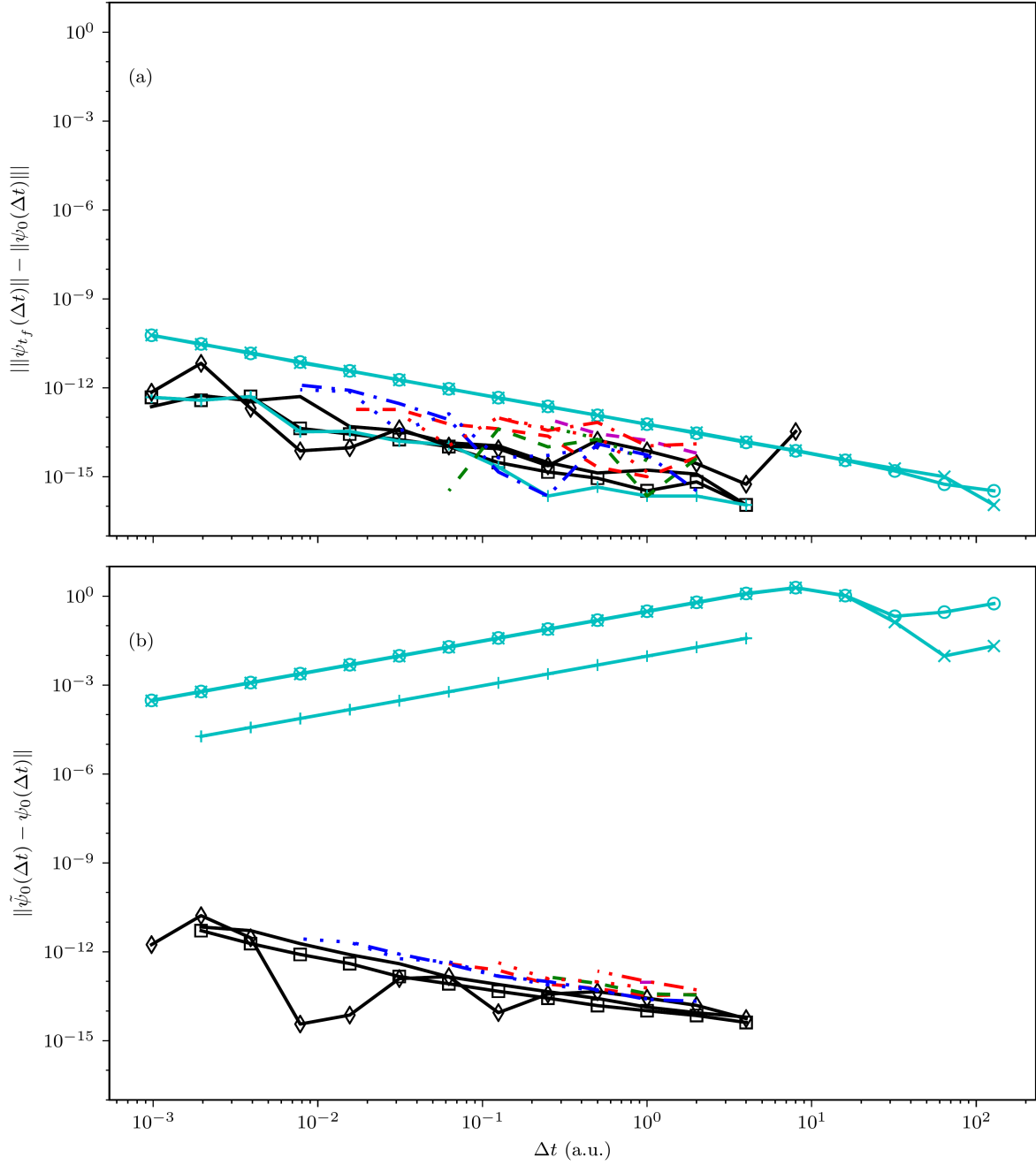


FIG. S4. Norm conservation (a) and time reversibility (b) of various integrators at the final time $t_f = 256$ a.u. as a function of the time step Δt used for the local energy control of retinal. Reversibility is measured as in Fig. 4 and line labels are the same as in Fig. S1.